Environmental Pollution 346 (2024) 123595

Contents lists available at ScienceDirect

Environmental Pollution

journal homepage: www.elsevier.com/locate/envpol

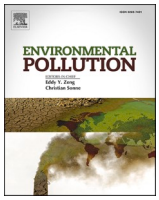

# Toxic effects and action mechanism of metal-organic framework UiO-66-$NH_2$ in *Microcystis aeruginosa*☆

Yiling Li [a,b], Wen-Xiong Wang [a,b,*]

[a] School of Energy and Environment and State Key Laboratory of Marine Pollution, City University of Hong Kong, Kowloon, Hong Kong, China
[b] Research Centre for the Oceans and Human Health, City University of Hong Kong Shenzhen Research Institute, Shenzhen, 518057, China

ARTICLE INFO

*Keywords:*
Metal organic framework
*Microcystis aeruginosa*
Toxicity
Algal organic matter
Metabolism

ABSTRACT

The zirconium metal-organic framework UiO-66-$NH_2$ has garnered considerable attention for their potentials of removing environmental contaminants from water. The production and application of UiO-66-$NH_2$ make their releases into the aquatic environment inevitable. Nevertheless, little information is available regarding its potential risk to the environment and aquatic organisms, thus limiting the evaluation of its safe and sustainable use. In this study, the ecotoxicity of UiO-66-$NH_2$ was evaluated, specifically its impacts on growth, extracellular organic matter release, and metabolomic changes of the model phytoplankton *Microcystis aeruginosa* (*M. aeruginosa*). UiO-66-$NH_2$ exhibited moderate effects on algal physiology including growth, viability, and photosynthetic system. At concentrations below 20 mg/L, UiO-66-$NH_2$ induced negligible inhibition of algal growth, algal viability, and photosynthesis. In contrast, UiO-66-$NH_2$ boosted the release of extracellular organic matter even at concentration as low as 0.02 mg/L. These findings indicated that, while no evident damage to algal cells was observed, UiO-66-$NH_2$ was hazardous to the aquatic environment as it stimulated the release of algal toxins. Moreover, UiO-66-$NH_2$ entered algal cells rather than adhering to the surface of *M. aeruginosa* as observed by the fluorescence imaging. Based on metabolic analysis, UiO-66-$NH_2$ influenced the cyanobacteria mainly through interference with purine metabolism and ABC transporter. This study sheds light on the potential threat UiO-66-$NH_2$ posing to microalgae, and has potential implications for its safe utilization in the environmental field.

## 1. Introduction

Metal-organic frameworks (MOFs), constructed from metal ions/clusters and organic linkers, are a new generation of porous hybrid materials that combine the merits of both organic and inorganic materials (Kitagawa, 2014). Among the numerous MOFs developed to date, zirconium terephthalate UiO-66 series MOF (where UiO stands for the University of Oslo) has received extensive attention in environmental contaminant adsorption and degradation due to its superior chemical and hydrothermal stability than most other MOFs (Ahmadijokani et al., 2022; Huang et al., 2017; Kandiah et al., 2010; Li et al., 2023; Mu et al., 2023; Zou and Liu, 2019; Rego et al., 2022). UiO-66 series MOF has been hailed as a potential MOF candidate for commercialization and large-scale applications (Hu and Zhao, 2015). A full understanding of the potential environmental threats associated with the release of UiO-66 series MOF into various ecosystems is of paramount importance before its commercialization (Orellana-Tavra et al., 2016; Ruyra et al., 2015; Yuan et al., 2022; Dymek et al., 2021). Functionalization of MOFs, such as amino-, nitro-, and carboxylate-, were found to exhibit superior performance than the pristine ones, extending their applicability in polar atmosphere and water treatment (Kim et al., 2021; Wu et al., 2020). Amines are a key chemical handle in MOF functionalization (Kim et al., 2021). Nanoscale UiO-66-$NH_2$ was reported to be moderately cytotoxic to HepG2 cells (Orellana-Tavra et al., 2016). A further study showed that UiO-66 particles could induce mild mechanical damage to fungi and the toxicity was low compared to other unstable MOF materials (Yuan et al., 2022). Despite these research efforts, knowledge about the threat of UiO-66-$NH_2$ to aquatic organisms remains scarce.

Algae are among the most vulnerable aquatic indicator organisms as they are sensitive to xenobiotics and form the base of the aquatic food

☆ This paper has been recommended for acceptance by Sarah Harmon.

* Corresponding author. School of Energy and Environment and State Key Laboratory of Marine Pollution, City University of Hong Kong, Kowloon, Hong Kong, China.
*E-mail address:* wx.wang@cityu.edu.hk (W.-X. Wang).

https://doi.org/10.1016/j.envpol.2024.123595
Received 26 November 2023; Received in revised form 15 February 2024; Accepted 15 February 2024
Available online 16 February 2024

chain (Gu et al., 2021; Monikh et al., 2021). Several pilot studies have examined the toxicological effects of MOFs on algae (Fan et al., 2019; Li et al., 2021; Zhang et al., 2021; Li et al., 2022). For example, Zeolitic imidazolate frameworks at concentrations of 0.01–1 mg/L were found to induce significant algal growth inhibition, chloroplast damage, and chlorophyll biosynthesis inhibition (Zhang et al., 2021). Although details regarding the threat of typical MOFs to algae have been reported, the potential effects of UiO-66-$NH_2$ have not been elucidated to date. Recent studies have shown that exposure to nanoparticles induced environmental risks by increasing the release of toxins into aquatic ecosystems during the growth and lysis of cyanobacterial cells, consequently posing a potential threat to algae-laden water (Fan et al., 2021; Xin et al., 2018). Algal toxins such as microcystin, proteins, and polysaccharose-like substances are typical constitutes of extracellular organic matter (EOM) produced by cyanobacteria ( Xin et al., 2018). Despite the prevailing concern raised by the toxicity of MOFs for aquatic organisms, knowledge about the influences of MOFs on the production of EOM and the exudation of algal toxins is still insufficient.

Metabolites are the end output of cellular biochemical activity (Patti et al., 2012). Information on alterations in metabolite profiles provides insight into the physiologic state of organisms (Nicholson et al., 2002). The use of metabolomics plays a vital role in research on specific toxicity pathways or molecular mechanisms induced by nanoparticle exposure (He et al., 2020; Huang et al., 2020). Generally, low exposure doses generate undetectable responses by measuring typical physiological endpoints, e.g., growth, photosynthesis, and lipid peroxidation (Holden et al., 2016; Liu et al., 2018). Metabolomics are sensitive and powerful tools that can capture the traditional “invisible” changes in organisms exposed to environmental concentrations of xenobiotics (Majumdar and Keller, 2020).

This study explored the biological/ecological impacts of UiO-66-$NH_2$ on the typical cyanobacterium *M. aeruginosa*. Interactions between UiO-66-$NH_2$ and *M. aeruginosa* were visualized *in situ* and the associated adverse effects were evaluated via algal growth inhibition, algal viability, and photosynthesis changes. Moreover, the environmental feedback after UiO-66-$NH_2$ came into contact with algae was clarified by determining the release of EOM into the aquatic environment in response to UiO-66-$NH_2$ stress. Furthermore, changes in metabolomics and related mechanisms resulting from UiO-66-$NH_2$ exposure were evaluated using untargeted metabolomics based on liquid chromatography-mass spectrometry. This work provides insight into the ecological risks UiO-66-$NH_2$ poses on aquatic organisms, which will be useful for evaluating their theoretical design and practical application.

## 2. Materials and methods

### 2.1. Synthesis and characterization of UiO-66-$NH_2$

UiO-66-$NH_2$ particles were prepared following procedures reported in the literature (Zhao et al., 2022). Briefly, $ZrCl_4$ and 2-aminoterephthalic acid were dissolved in 50 mL dimethylformamide to achieve final concentrations of 1 mmol. Then, 6 mL of acetic acid was added into the above solution. The mixture was reacted at 120 °C for 24 h in Teflon-lined autoclave. The obtained products were centrifuged, washed with methanol several times and dried in a vacuum oven. The morphology of these UiO-66-$NH_2$ particles were characterized by transmission electron microscopy (Philips CM20). Powder X-ray diffraction (PXRD) data of as-synthesized UiO-66-$NH_2$ particles were collected on a Malvern Panalytical Xpert 3 X-ray diffractometer equipped with a Cu anode of 1.5406 Å λ radiation. Fourier transform infrared spectroscopy (Shimadzu, Japan) was used to screen for the presence of various functional groups in the as-synthesized UiO-66-$NH_2$ particles. The Fourier transform infrared spectroscopy assay was conducted in transmission mode with a spectral range of 4000–500 $cm^{-1}$. Zeta potentials and hydrodynamic diameters of as-synthesized UiO-66-$NH_2$ particles were determined by the dynamic light scattering (DLS, ZetaPlus, Brookhaven, USA).

### 2.2. Algal cultivation and MOF exposure

*M. aeruginosa* was purchased from the Institute of Hydrobiology, Chinese Academy of Science, and cultivated in sterile BG11 medium (pH = 8.1 ± 0.1) with a 16/8 h light/dark cycle as described previously (Li et al., 2022). Stock solutions (4 mg/mL) of as-synthesized UiO-66-$NH_2$ were prepared by dispersing them in water through sonication in a water bath for 30 min. Exponentially grown *M. aeruginosa* were harvested by centrifugation at 3000 rpm for 10 min and then suspended in BG11 media to obtain a specific final concentration of $2 \times 10^5$ cells/mL. In the case of physiological endpoints assay, different volumes of UiO-66-$NH_2$ stock solutions were added to the algal solution to reach concentrations ranging from 1 mg/L to 100 mg/L. The mixtures were then maintained under algal culture conditions for 72 h.

### 2.3. Algal growth inhibition, cell viability test, and photosynthesis

At the end of exposure, algal cell numbers were counted using flow cytometry (FACSAria™ III sorter, BD, San Josa, CA USA) to determine the growth inhibitory effect induced by UiO-66-$NH_2$. The cell viability of *M. aeruginosa* was tested using a time-resolved Fluorescein diacetate-based method as described previously (Li et al., 2022). Briefly, 10 μL of 10 mg/L Fluorescein diacetate and 190 μL of algal solutions were added into a 96-well plate. The resulting fluorescence signals derived from the enzymatic hydrolysis of Fluorescein diacetate by live cells were measured at Ex 485 nm/Em 525 nm within 30 min. The slope of the curve, which is directly proportional to cell viability, was then used to assess algal viability. The photosynthetic performance of *Microcystis* cells after UiO-66-$NH_2$ treatment was monitored by Imaging-PAM M-series Maxi Version (WALZ, Effeltrich, Germany) using $F_v/F_m$ as indicator.

### 2.4. Chemical stability of as-synthesized MOF materials

The stabilities of as-synthesized UiO-66-$NH_2$ particles toward algal culture medium were assessed by dispersing them in BG11 medium and incubating them under conditions similar to those used for algal culture. After various incubation times, samples were collected by centrifugation at 7000 rpm for 12 min, followed by ultrafiltration and digestion with concentrated nitric acid. Inductively coupled plasma mass spectrometry (NexION 300X, PerkinElmer, USA) was then used to quantify Zr. Based on the release percentage of UiO-66-$NH_2$ particles in BG11 medium, the algae were exposed to the metal ions (Zr) and organic linkers (2-aminoterephthalic acid) as described above. The algal growth inhibition was used as toxicological endpoint to study the algal toxic effects of the released metal ions and linkers.

### 2.5. UiO-66-$NH_2$ uptake by microcystis cells

To reveal the internalization of UiO-66-$NH_2$ particles in *M. aeruginosa* cells, the algae were treated with rhodamine (RhB) labeled UiO-66-$NH_2$ particles and further visualized using flow cytometry and confocal laser scanning microscopy (LSM900 with Airyscan2, Zeiss, Germany). UiO-66-$NH_2$-RhB was synthesized following the method reported by Gao et al. (2018) with minor modifications. Briefly, 2 mg of UiO-66-$NH_2$ was dispersed in 2 mL of 2 mM RhB aqueous solutions by sonication for 30 min. After incubation overnight, the mixtures were centrifuged and washed several times with ultrapure water until no RhB could be detected in the supernatant. The powder thus obtained was regarded as UiO-66-$NH_2$-RhB. The optical properties of the obtained UiO-66-$NH_2$-RhB were recorded on a UV-VIS Spectrophotometer (UV3600, Shimadzu). As shown in Fig. S1, UiO-66-$NH_2$-RhB presented two well-separated emission peaks at 430 nm and 585 nm, corresponding to UiO-66-$NH_2$ and RhB molecule, respectively.

*M. aeruginosa* cells were harvested and exposed to 1–100 mg/L of UiO-66-$NH_2$-RhB as described above. After 72 h exposure, the algae from both the control and UiO-66-$NH_2$-RhB treated groups were collected and washed three times with phosphate buffered saline to remove surface adsorbed UiO-66-$NH_2$-RhB. The SSC values of 10,000 Microcystis cells with or without UiO-66-$NH_2$-RhB treatment was determined by flow cytometry. The uptake of UiO-66-$NH_2$-RhB was expressed as the SSC values of MOF treated algae/control algae × 100%. To visualize the internalization of UiO-66-$NH_2$-RhB in *Microcystis* cells, *M. aeruginosa* were incubated with 20 mg/L UiO-66-$NH_2$-RhB for 24 h. The mixtures were collected and fixed with 1% glutaraldehyde for 10 min. Then, the algae were analyzed using a confocal laser scanning microscopy to visualize the interactions between *M. aeruginosa* and UiO-66-$NH_2$-RhB. For UiO-66-$NH_2$-RhB imaging, excitation and emission wavelengths were set to 561 nm and 580–600 nm, respectively. For *M. aeruginosa* autofluorescence, excitation and emission wavelength were set to 633 nm and 650–700 nm, respectively.

### 2.6. EOM extraction and analysis

EOM was extracted from *M. aeruginosa* cells after treatment with UiO-66-$NH_2$ for 72 h. After centrifugation (5000 rpm, 10 min), the supernatant was collected and filtered through 0.45 μm cellulose acetate membranes to obtain the EOM. Fluorescence excitation-emission matrices of the collected EOMs were obtained on a fluorescence spectrophotometer with an excitation range of 230–650 nm at 10 nm intervals and an emission range of 230–780 nm at 1 nm intervals.

### 2.7. Metabolism

After exposure to UiO-66-$NH_2$ for 72 h, the algal suspension (5 mL) was centrifuged at 5000 rpm for 8 min to harvest cells. The collected cells were then washed twice with ice-cold phosphate buffered saline, and snap-frozen in liquid nitrogen. To extract the metabolites, 0.8 mL of precooled extraction reagent (methanol:$H_2O$, 70:30, v/v) were added to the cells. The mixtures were homogenizing for 5 min using TissueLyser (JXFSTPRP, China) and sonicated for 30 min at 4 °C. The samples were incubated at −20 °C for 1 h, followed by centrifugation at 14,000 for 15 min. The supernatant was collected, filtered through 0.22 μm microfilters, and transferred to autosampler vials for subsequent analysis. Quality control samples were prepared by pooling equal aliquots of each sample from control and UiO-66-$NH_2$ treatment group. Metabolite profiling of *M. aeruginosa* was performed on an ultrahigh performance liquid chromatography (Waters ACQUITY, USA) coupled to a Q-Exactive mass spectrometer (ThermoFisher Scientific, USA). A Hypersil GOLD aQ column (Thermo Fisher Scientific, USA) was used for chromatographic separation. A heated electrospray ionization (HESI) source was used for mass detection. The data was acquired in both positive and negative ionization modes. The details are provided in the Supporting Information.

### 2.8. Statistical analysis

All data are expressed as mean ± standard deviation of at least three replicates. One-way analysis of variance was utilized to analyze the statistical significance among different groups, where $P < 0.05$ was considered to indicate significant differences.

## 3. Results and discussion

### 3.1. Characterization of UiO-66-$NH_2$ particles

The PXRD pattern of as-synthesized UiO-66-$NH_2$ is displayed in Fig. 1A. The sharp peaks shown in the PXRD patterns of as-synthesized UiO-66-$NH_2$ indicated strong crystallinity. The diffraction patterns matched those reported in the literature well, with three distinct peaks at $2\theta = 7.34$, 8.46, and 25.66° (Hou et al., 2015). All observed $2\theta$ peaks matched the calculated pattern, indicating that no impurities were present in the crystalline structure. As shown by the TEM micrograph, as-synthesized UiO-66-$NH_2$ had a cubic shape with a crystal size of around 150 nm (Fig. 1B and C). The as-synthesized products were further characterized by Fourier transform infrared spectroscopy in the near infrared region of 4000–500 $cm^{-1}$, allowing the identification of the organic ligands present in UiO-66-$NH_2$ particles (Fig. 1D). As shown in Fig. 1E, the hydrodynamic diameter of UiO-66-$NH_2$ was ~250 nm and exhibited no significant change over the 72-h experimental period, indicating that UiO-66-$NH_2$ was stable in BG11 medium. UiO-66-$NH_2$ was negatively charged in the medium with an absolute value of −24.7

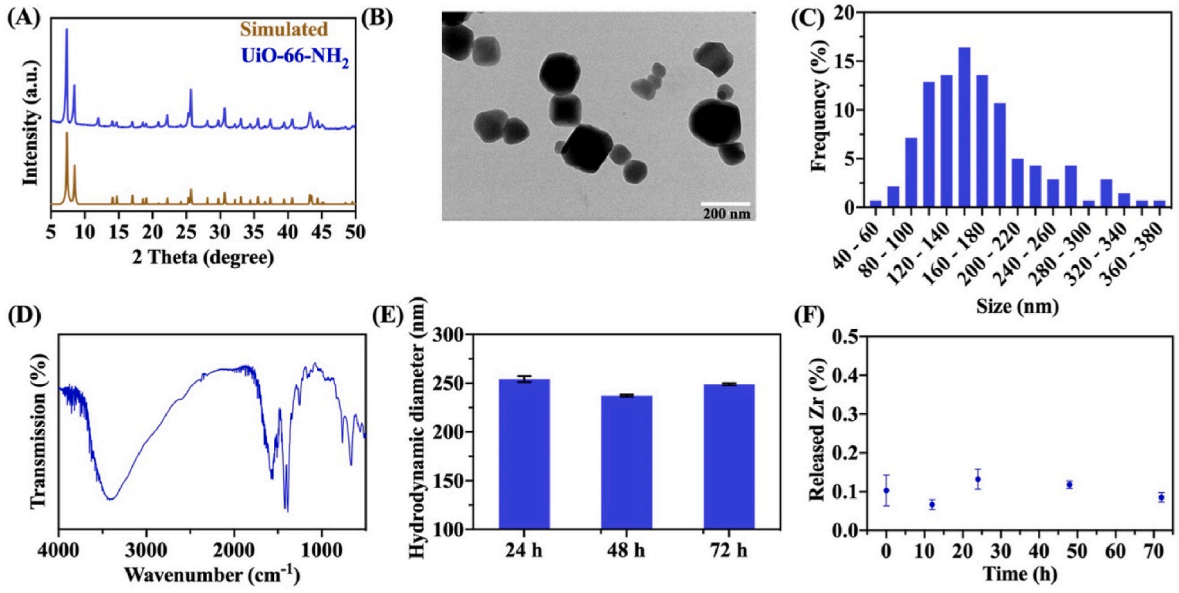


**Fig. 1.** Characterization of UiO-66-$NH_2$. (A) Powder X-ray diffraction pattern of UiO-66-$NH_2$. (B) Transmission electron microscopic image and (C) particle size distribution of UiO-66-$NH_2$. (D) Fourier transform infrared spectra of UiO-66-$NH_2$. (E) Hydrodynamic diameters of UiO-66-$NH_2$ in BG11 medium. (F) Zr released from UiO-66-$NH_2$ over 72 h.

mV, indicating the high dispersivity of UiO-66-$NH_2$ particles. During exposure period, the algal solutions were shaken twice daily by hand to promote contact between UiO-66-$NH_2$ particles and *M. aeruginosa* cells. The aqueous stabilities of UiO-66-$NH_2$ were evaluated by measuring the released $Zr^{4+}$ in BG11 medium. Metal ion release from UiO-66-$NH_2$ particles was limited throughout the exposure period (<0.2%), confirming their high aqueous stabilities (Fig. 1F). Taken together, these findings show that UiO-66-$NH_2$ was uniformly dispersed and highly stable in the BG11 matrix.

### 3.2. Algal physiological responses to UiO-66-$NH_2$

Several physiological endpoints, including algal growth, viability, and photosynthesis were used to assess the potential toxicological impacts of UiO-66-$NH_2$ on *M. aeruginosa*. To the best of our known, until now, there are no reports about the factual concentrations of MOFs in the environment. UiO-66-$NH_2$ at concentrations ranging from dozens to hundreds mg/L were commonly used in environmental remediation research. Herein, to provide information about the biosafety use of MOFs and their environmental risk assessment, UiO-66-$NH_2$ at dosages ranging from one-tenths to dozens mg/L was utilized. Fig. 2A depicts the dose-dependent algal growth inhibition of UiO-66-$NH_2$ on *M. aeruginosa*. The calculated 72 h $EC_{50}$ value was 44 mg/L. No significant growth inhibitory effect was detected at a concentration of UiO-66-$NH_2$ below 1 mg/L. At the highest exposure dosage (100 mg/L), UiO-66-$NH_2$ induced 83% growth inhibition on *M. aeruginosa*. The algal inhibitory effect of UiO-66-$NH_2$ was lower than that of other MOFs, such as Cu-MOFs and Zn-MOFs. At dosages above 1 mg/L, Cu-MOF-74 presented growth inhibitory effects to *M. aeruginosa* by 372%, and this growth inhibition was basically due to intracellular reactive oxygen species and $Cu^{2+}$ released from MOF particles (Fan et al., 2019; Yue et al., 2023). Zeolitic imidazolate frameworks at concentrations of 0.01–1 mg/L were reported to induce significant nanotoxicity including algal growth inhibition, chloroplast damage, and chlorophyll biosynthesis (Zhang et al., 2021). Regarding algal viability, the tested $EC_{50}$ was 15 mg/L for UiO-66-$NH_2$ (Fig. 2B). In *M. aeruginosa*, photosynthesis (reflected by $F_v/F_m$ ratios) was inhibited by 72 h under ≥20 mg/L UiO-66-$NH_2$ treatment. The algal toxicity of UiO-66-$NH_2$ was compared to that of pristine UiO-66 to evaluate the contribution of reactive amine groups from organic linkers. The successful synthesis of UiO-66 was confirmed by XRD pattern and fourier transform infrared spectra (Fig. S2). UiO-66 displayed more-negative zeta potentials (−35.9 ± 4.9 mV) in comparison with UiO-66-$NH_2$. Previous studies have revealed that surface modification with amine groups promoted the interaction between nanoparticles and microalgal cells (Li et al., 2022; Wang et al., 2013). As shown in Fig. S3, UiO-66-$NH_2$ displayed much higher inhibition on algal growth, algal cell viability and photosynthesis than UiO-66 did. Obviously, the amine groups existing on the surface of UiO-66-$NH_2$ MOFs contributed to their enhanced toxic effects than pristine MOFs. Metal ions have been reported to be released from metal nanoparticles and then pose additional toxicity to organisms (Tortella et al., 2020). Herein, $ZrCl_2$ and 2-aminoterephthalic acid was utilized to assess the toxic effects of the released metal ions and organic linkers on algae. As indicated by cell density test, the metal ions ($Zr^{4+}$) and organic linkers (2-aminoterephthalic acid) had no obvious toxic effects on *M. aeruginosa* (Fig. S4). Therefore, it can be concluded that the algal toxicity was due to the UiO-66-$NH_2$ particles rather than the metal ions or organic linkers released from them. Similar results were reported for certain water-stable MOF particles such as MIL-101(Cr) and porphyrin MOF (Li et al., 2021). However, the released metal ions were regarded as the main cause of toxicity induced by the water unstable MOFs, such as Cu-MOF (Fan et al., 2019; Li et al., 2021). In general, utilizing algal growth, cell viability and photosynthesis as toxicity endpoints, the tested Zr-based UiO-66-$NH_2$ MOF showed better biocompatibility than other previously reported types of MOFs.

### 3.3. Internalization of UiO-66-$NH_2$ inside M. aeruginosa cells

Direct physical effects are the well-accepted mechanisms for growth suppression and metabolic disturbance in algal cells (Malina et al., 2019). Nanomaterials were shown to interact with the cell wall, agglomerate on the algal surface, and consequently induce toxicity (Monikh et al., 2020). According to the results of confocal imaging, UiO-66-$NH_2$-RhB was not found to adhere to the algal surface (Fig. 3). These results indicated that the damage of UiO-66-$NH_2$ to algae did not result from direct physical contact. The observed adverse effect of UiO-66-$NH_2$ was inconsistent with other MOF materials such as MIL-101, which are tightly attached to the outer surface of algae (Li et al., 2022). In addition to adsorption, cellular internalization of nanomaterials was another toxic mechanism that contributed to the toxicity caused by other nanomaterials including silver nanomaterials, quantum dots, and carbon-based nanomaterials (Al-Shaeri et al., 2022; Huang et al., 2019; Yan et al., 2022). The side scatter (SSC) value reflected the complexity of cells and has recently been used as an indicator for evaluating the contents of nanoparticles inside cells (Garcia Romeu et al., 2021). Herein, the SSC value of flow cytometry was used to quantitatively examine the internalization of UiO-66-$NH_2$ inside *M. aeruginosa*(Fig. S5). Compared to that of control algae, the SSC intensity of *M. aeruginosa* increased by 1.09, 1.12, 1.21, and 1.17 times under 5, 20, 50, and 100 mg/L of UiO-66-$NH_2$ exposure, respectively (Fig. S5). The dose-dependent increase in SSC reflected a dose-dependent bioaccumulation of UiO-66-$NH_2$ by *M. aeruginosa*, which was corrected with the dose-dependent toxicity to *M. aeruginosa* caused by UiO-66-$NH_2$. The slight reduction in the SSC value in the 100 mg/L group may be due to the breakage of algal cells and the resulting loss of intracellular accumulated UiO-66-$NH_2$ particles. To further elucidate the internalization of UiO-66-$NH_2$ in *M. aeruginosa* cells, UiO-66-$NH_2$ particles were labeled with the fluorescent dye RhB (Fig. S1). Representative images of *M. aeruginosa* cells treated with 20 mg/L of RhB labeled UiO-66-$NH_2$ for 24-h are presented in Fig. 3. The 3D image clearly shows yellow dots in the cellular context of *M. aeruginosa*, indicating the accumulation of UiO-66-$NH_2$ particles or aggregates inside *M. aeruginosa* cells. No fluorescence signal was detected in the *M. aeruginosa* treated with RhB alone (Fig. S6). Because

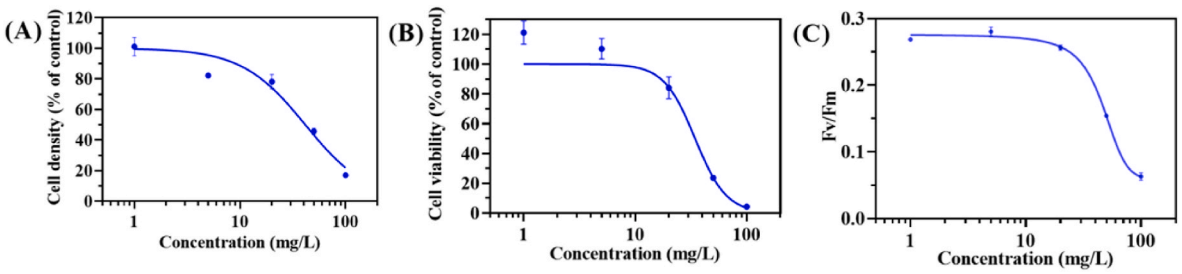


**Fig. 2.** Toxicity of *Microcystis* cells exposed to UiO-66-$NH_2$. (A) *Microcystis* cell density, (B) *Microcystis* cell viability, and (C) $F_v/F_m$ value of *Microcystis* cells exposed to UiO-66-$NH_2$ for 72 h.

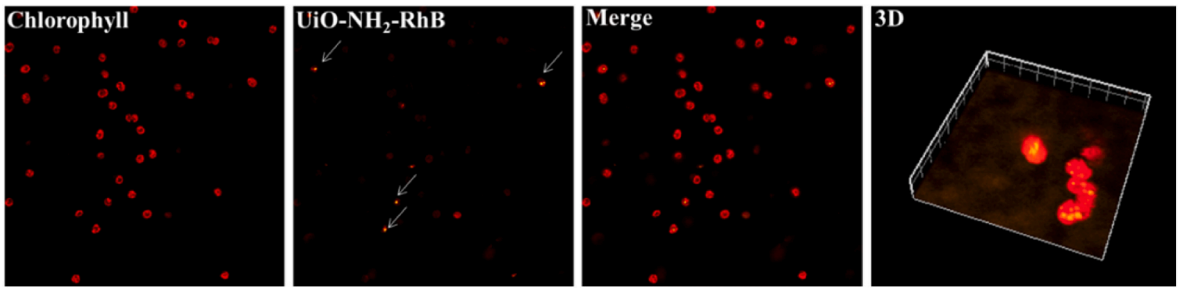


**Fig. 3.** Confocal imaging of UiO-66-$NH_2$-RhB treated *Microcystis* cells. Images of *Microcystis* cells showing chlorophyll autofluorescence and subcellular distribution of UiO-66-$NH_2$-RhB.

of the inability to image all algal cells by confocal microscopy, a total of 500 microalgae were randomly selected to assess the internalization efficiency of UiO-66-$NH_2$ by *M. aeruginosa* cells. The results of quantitative image analysis indicated that not all *M. aeruginosa* cells accumulated UiO-66-$NH_2$-RhB; such accumulation only occurred in 10% of algal cells. The superiorities of fluorescent imaging are based on the simplicity of the synthesis and imaging procedure of dye-labeled nanoparticles. Nevertheless, the photodegradation and leaching out of fluorescent dye in the imaging experiments need more studies. Besides, TEM images are alternative ways to verify the absorbed and internalized nanoparticles inside cells. Taken together, the internalization of UiO-66-$NH_2$ in the cellular compartment of *M. aeruginosa* may be one of the causes for the inhibitory effect of UiO-66-$NH_2$ on physiological dysfunction.

### 3.4. Low dosage of UiO-66-$NH_2$ promoted the release of EOM

The EOM compositions of *M. aeruginosa* under UiO-66-$NH_2$ treatment were analyzed by 3D excitation-emission matrix spectroscopy analysis (Fig. 4). Three distinct fluorescence components—assigned to tryptophan/protein-like substances, humic-like substances, and fulvic-like substances—were observed in the EOM of *M. aeruginosa*. The intensities of the relevant fluorescence peaks under given conditions are summarized in Table S1. UiO-66-$NH_2$ showed minimal influence (<10% reduction) on the formation of tryptophan/protein-like organic components and the enhanced formation was <10% even when the dosage was increased to 50 mg/L (Fig. 4 and Fig. S7). The inconspicuous fluorescence changes of tryptophan/protein-like organics after UiO-66-$NH_2$ treatment suggest that *Microcystis* cells under UiO-66-$NH_2$ exposure grow well and have a strong metabolism. The unchanged intensity of tryptophan/protein-like substances matched the unchanged cell viability and photosynthesis discussed above. Unlike tryptophan/protein-like substances, fluorescence intensities of humic and fulvic-like components increased with increasing UiO-66-$NH_2$ dosage. UiO-66-$NH_2$ dramatically promoted their formation, resulting in 800- and 2000-fold increases even at 1 mg/L. Even if the exposure dosage of UiO-66-$NH_2$ was as low as 0.02 mg/L, a remarkable increase of humic- and fulvic-like substances (by 2-fold) was detected (Fig. 4). Biological activity was reported as one of the major factors engaged in humic-like substances formation (Qu et al., 2012). The reasons for the observed phenomenon mainly due to the fact that low concentrations of UiO-66-$NH_2$ promoted the biological activity of *M. aeruginosa*, and subsequently stimulated the algae to release EOM. This result was consistent with increased cell viability under low concentrations of UiO-66-$NH_2$ treatment. Humic acid contains many active functional groups (e.g., carboxyl, hydroxyl, carbonyl, quinone, and methoxy group), and is considered as the primary culprit of membrane fouling (Zhang et al., 2018). As the major precursors of disinfection byproducts of algal cells, humic and fulvic acid contained in EOM pose a serious threat to the safety of drinking water and human health. The presence of as little as 0.05 mg/L UiO-66-$NH_2$ in algae-laden water will promote the release of humic- and fulvic-like substances, therefore posing a substantial threat to aquatic safety. Thus, even though at mg/L levels, UiO-66-$NH_2$ exhibited no harmful effects to algae itself in case of physiological endpoints, the risk of aquatic ecotoxicity still exists because of the leached harmful EOM component.

### 3.5. Metabolic responses of *M. aeruginosa* to UiO-66-$NH_2$ exposure

The physiological responses presented above indicated that only higher doses of UiO-66-$NH_2$ (dozens of mg/L level) caused variations in biochemical end points within 72 h (e.g., growth inhibition and reduction in cell viability). Nevertheless, although no detectable influence on physiology perturbations was observed, UiO-66-$NH_2$ induced significantly elevated EOM release at concentrations as low as 0.05 mg/L, suggesting metabolic reprogramming of *M. aeruginosa*. Herein, based on nontargeted liquid chromatography-mass spectrometry, metabolomics was performed to disclose invisible changes in *M. aeruginosa* at metabolite levels exposed to low concentrations of UiO-66-$NH_2$.

A total of 123 metabolites were identified and quantified in

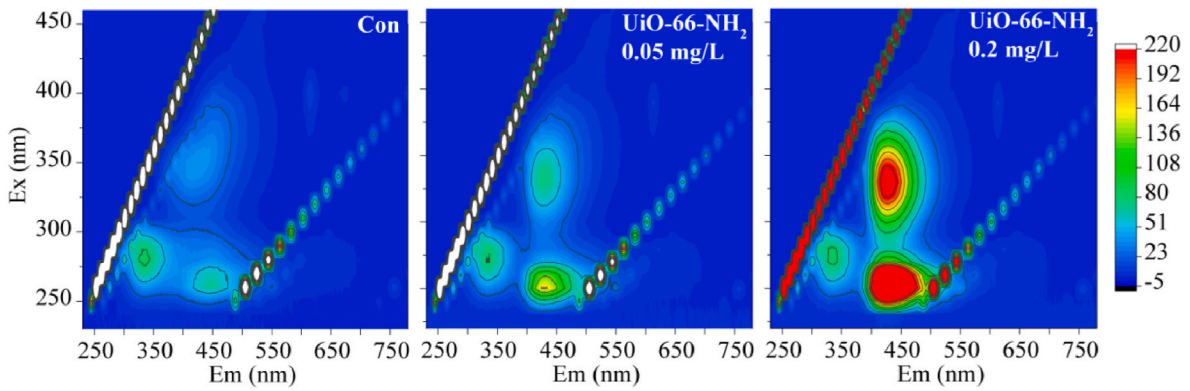


**Fig. 4.** Excitation-emission matrices of extracellular organic matter of the control, 0.05 mg/L, and 0.2 mg/L of UiO-66-$NH_2$ treated groups.

*M. aeruginosa*. Fig. 5A presents general metabolite changes in UiO-66-$NH_2$ treated algae versus control algae, represented by volcano plots. Partial least-squares-discriminant analysis (PLS-DA) was performed to acquire a holistic view of how the metabolite profile changed in response to the UiO-66-$NH_2$ treatment. The PLS-DA score plot indicated clear separation of the UiO-66-$NH_2$ group from the control group, showing a high discrimination with an explanation ratio ($R^2Y$) above 0.99 and a predictive power ($Q^2$) above 0.7 (Fig. 5B). These data indicated that even low concentrations of UiO-66-$NH_2$ altered the normal metabolic profile of *M. aeruginosa*, although no detectable physiological responses were observed. A similar finding was obtained in algae under toxic metal and metal nanoparticle stress (Huang et al., 2020; Slaveykova et al., 2021). Slaveykova et al. found that metabolites respond faster to mercury exposure than algal physiology. They suggested the potential utilization of metabolomics to disclose biological effects at low toxicant levels and at an early stage of exposure.

A total of 22 metabolites (6 upregulated and 16 downregulated) were found to be significantly regulated by UiO-66-$NH_2$ after comparison to the control groups ($p < 0.05$). The detailed metabolite information is listed in Table S2. These significantly regulated metabolites were classified into six categories including (I) endogenous metabolites, (II) amino acids, peptides, and analogues, (III) fatty acyls [FA], (IV) alkaloids, (V) carbonyl compounds, and (VI) others. Among all UiO-66-$NH_2$ regulated metabolites, 32% belonged to category I (endogenous metabolites) and 23% belonged to category II (amino acids, peptides, and analogues). Amino acids and carbonyl compounds metabolism were also found to be undermined by other nanoparticles such as $TiO_2$ and $MoS_2$ (Yuan et al., 2018). Exposure to $MoS_2$ resulted in increased amino acid levels in the green microalga *Chlorella vulgaris*. The biological pathways regulated by these dysregulated metabolites are interpreted in Fig. 5C. The responsive metabolites under UiO-66-$NH_2$ treatment correspond to enriched pathways that are specific to purine metabolism and ATP-binding cassette (ABC) transporters. Metabolites including L-(+)-Arginine, α-Lactose, and adenosine are enriched in the metabolic pathway of ABC transporters. In algae, ABC transporters that reside in membranes of diverse organelles mediate various biological processes, such as resistance to environmental stimuli and transport of endogenous secondary metabolites. Specially, they are strongly involved in both the export and import of substrates (e.g., amino acids, nucleotides, carbohydrates, lipids, proteins, and other metabolites) across membranes. The observed upregulation of ABC transporters indicated that the transport of endogenous toxins and metabolites was active in *M. aeruginosa* under UiO-66-$NH_2$ stress. This agrees with the observation of the high release of EOM in UiO-66-$NH_2$ treated *M. aeruginosa*. Artificial nanomaterials such as titanium dioxide nanoparticles, polystyrene microplastics, copper oxide, and zinc oxide nanomaterials resulted in enrichment of different metabolites in the ABC transporter pathway (Liu et al., 2022; Wang et al., 2023; Wu et al., 2015; Xiong et al., 2022).

In the present study, the observed upregulation of the ABC transporter pathway suggested that transmembrane transport was active (Wang et al., 2023). The downregulation of metabolites in the purine metabolism pathway suggested that the purine metabolism could be inhibited by UiO-66-$NH_2$ in *M. aeruginosa*. Considering that purines are essential components of nucleic acids, alteration of the purine metabolism indicates a disorder of DNA replication or transcription in algae induced by UiO-66-$NH_2$ (You et al., 2021). Considering that the amino acids serve as precursors for a wide variety of metabolites, the inhibited purine metabolism agrees with the amino acid downregulation described above (Batista-Silva et al., 2019). Overall, the present study shows the information on the metabolic perturbations in cyanobacterium *M. aeruginosa* in response to UiO-66-$NH_2$. These findings indicate that the regulation of the ABC transporter and the observed inhibition of the purine metabolism could be vital mechanisms responsible for the defense of *M. aeruginosa* to damage from UiO-66-$NH_2$ at low levels.

## 4. Conclusion

As a superior water-stable MOF, UiO-66-$NH_2$ has aroused great attention for the removal of environmental pollutants from water. This enables substantial cyanobacterial interaction with UiO-66-$NH_2$ particles during their use and disposal. In this study, the impacts of UiO-66-$NH_2$ on cyanobacteria *M. aeruginosa* were systematically examined using

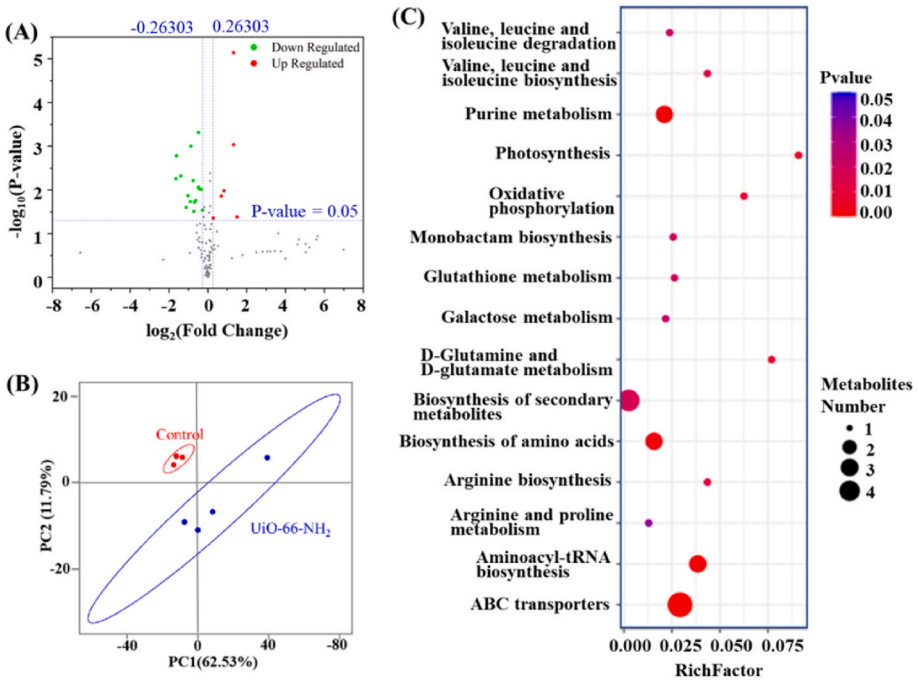


**Fig. 5.** Metabolic analysis of *M. aeruginosa* exposed to UiO-66-$NH_2$ particles. (A) Volcano plots displaying up- and down-regulated metabolites compared to control algae. (B) Partial least-squares-discriminant analysis score plot of metabolic profiles of *M. aeruginosa* treated with and without UiO-66-$NH_2$. (C) Significantly disturbed pathways in *M. aeruginosa* influenced by UiO-66-$NH_2$.

typical physiological endpoints, including cell density, cell viability, photosynthesis, and EOM release. Alterations of the metabolite profile of *M. aeruginosa* under UiO-66-$NH_2$ treatment were evaluated. UiO-66-$NH_2$ induced physiological responses at high concentrations (>dozens of mg/L), which are commonly used in environmental remediation applications. These effects were partially caused by the internalization of UiO-66-$NH_2$ into cells. Below the harmful effect threshold to algae, UiO-66-$NH_2$ reprogrammed intracellular metabolism profiles and thus poses a threat to the aquatic environment via enhanced release of harmful EOM. These findings have critical implications for a better understanding of the interaction between UiO-66-$NH_2$ particles and primary producer microalgae. The present study highlights the importance to consider toxicity end points when assessing the environmental risks of artificial particles.

## CRediT authorship contribution statement

**Yiling Li:** Writing – original draft, Investigation, Formal analysis, Data curation, Conceptualization. **Wen-Xiong Wang:** Writing – review & editing, Supervision, Resources, Project administration, Funding acquisition, Conceptualization.

## Declaration of competing interest

The authors declare that they have no known competing financial interests or personal relationships that could have appeared to influence the work reported in this paper.

## Data availability

Data will be made available on request.

## Appendix A. Supplementary data

Supplementary data to this article can be found online at https://doi.org/10.1016/j.envpol.2024.123595.

## References


Ahmadijokani, F., Molavi, H., Rezakazemi, M., Tajahmadi, S., Bahi, A., Ko, F., Aminabhavi, M., Tejraj, Li, J.-R., Arjmand, M., 2022. UiO-66 metal organic frameworks in water treatment: a critical review. Prog. Mater. Sci. 125, 100904.

Al-Shaeri, M., Paterson, L., Stobie, M., Cyphus, P., Hartl, M., 2022. Trophic transfer of single-walled carbon nanotubes at the base of the food chain and toxicological response. Nanomaterials 12, 4363.

Batista-Silva, W., Heinemann, B., Rugen, N., Nunes-Nesi, A., Araújo, W.L., Braun, H.P., Hildebrandt, T., 2019. The role of amino acid metabolism during abiotic stress release. Plant Cell Environ. 42, 1630–1644.

Dymek, K., Kurowski, G., Kuterasiński, Ł., Jędrzejczyk, R., Szumera, M., Sitarz, M., Pajdak, A., Kurach, Ł., Boguszewska-Czubara, A., Jodłowski, P.J., 2021. In search of effective UiO-66 metal–organic frameworks for artificial kidney application. ACS Appl. Mater. Interfaces 13, 45149–45160.

Fan, G., Bao, M., Zheng, X., Hong, L., Zhan, J., Chen, Z., Qu, F., 2019. Growth inhibition of harmful cyanobacteria by nanocrystalline Cu-MOF-74: efficiency and its mechanisms. J. Hazard Mater. 367, 529–538.

Fan, G., Chen, Z., Yan, Z., Du, B., Pang, H., Tang, D., Luo, J., Lin, J., 2021. Efficient integration of plasmonic Ag/AgCl with perovskite-type $LaFeO_3$: enhanced visible-light photocatalytic activity for removal of harmful algae. J. Hazard Mater. 409, 125018.

Gao, N., Huang, J., Wang, L., Feng, J., Huang, P., Wu, F., 2018. Ratiometric fluorescence detection of phosphate in human serum with a metal-organic frameworks-based nanocomposite and its immobilized agarose hydrogels. Surf. Sci. 459, 686–692.

Garcia Romeu, H., Deville, S., Salvati, A., 2021. Time-and space resolved flow cytometry of cell organelles to quantify nanoparticle uptake and intracellular trafficking by cells. Small 17, 2100887.

Gu, W., Li, X., Du, M., Ren, Z., Li, Q., Li, Y., 2021. Identification and regulation of ecotoxicity of polychlorinated naphthalenes to aquatic food Chain (green algae-Daphnia magna-fish). Aquat. Toxicol. 233, 105774.

He, E., Qiu, R., Cao, X., Song, L., Peijnenburg, W.J., Qiu, H., 2020. Elucidating toxicodynamic differences at the molecular scale between ZnO nanoparticles and $ZnCl_2$ in *Enchytraeus crypticus* via nontargeted metabolomics. Environ. Sci. Technol. 54, 3487–3498.

Holden, P.A., Gardea-Torresdey, J.L., Klaessig, F., Turco, R.F., Mortimer, M., Hund-Rinke, K., Cohen Hubal, E.A., Avery, D., Barcelo, D., Behra, R., Cohen, Y., Deydier-Stephan, L., Ferguson, P.'L., Fernandes, T.F., Herr Harthorn, B., Henderson, W.M., Hoke, R.A., Hristozov, D., Johnston, J.M., Kane, A.B., Kapustka, L., Keller, A.A., Lenihan, H.S., Lovell, W., Murphy, C.J., Nisbet, R.M., Petersen, E.J., Salinas, E.R., Scheringer, M., Sharma, M., Speed, D.E., Sultan, Y., Westerhoff, P., White, J.C., Wiesner, M.R., Wong, E.M., Xing, B., Steele Horan, M., Godwin, H.A., Nel, A.E., 2016. Considerations of environmentally relevant test conditions for improved evaluation of ecological hazards of engineered nanomaterials. Environ. Sci. Technol. 50, 6124–6145.

Hou, J., Luan, Y., Tang, J., Wensley, A.M., Yang, M., Lu, Y., 2015. Synthesis of UiO-66-$NH_2$ derived heterogeneous copper(II) catalyst and study of its application in the selective aerobic oxidation of alcohols. J. Mol. Catal. Chem. 407, 53–59.

Hu, Z., Zhao, D., 2015. De facto methodologies toward the synthesis and scale-up production of UiO-66-type metal–organic frameworks and membrane materials. Dalton Trans. 44, 19018–19040.

Huang, X., Liu, Q., Yao, S., Jiang, G., 2017. Recent progress in the application of nanomaterials in the analysis of emerging chemical contaminants. Anal. Methods 9, 2768–2783.

Huang, B., Wei, Z.-B., Yang, L.-Y., Pan, K., Miao, A.-J., 2019. Combined toxicity of silver nanoparticles with hematite or plastic nanoparticles toward two freshwater algae. Environ. Sci. Technol. 53, 3871–3879.

Huang, M., Keller, A.A., Wang, X., Tian, L., Wu, B., Ji, R., Zhao, L., 2020. Low concentrations of silver nanoparticles and silver ions perturb the antioxidant defense system and nitrogen metabolism in $N_2$-fixing cyanobacteria. Environ. Sci. Technol. 54, 15996–16005.

Kandiah, M., Nilsen, M.H., Usseglio, S., Jakobsen, S., Olsbye, U., Tilset, M., Larabi, C., Quadrelli, E.A., Bonino, F., Lillerud, K.P., 2010. Synthesis and stability of tagged UiO-66 Zr-MOFs. Chem. Mater. 22, 6632–6640.

Kim, D., Kang, M., Ha, H., Hong, C.S., Kim, M., 2021. Multiple functional groups in metal–organic frameworks and their positional regioisomerism. Coord. Chem. Rev. 438, 213892.

Kitagawa, S., 2014. Metal–organic frameworks (MOFs). Chem. Soc. Rev. 43, 5415–5418.

Li, Y., Shang, S., Shang, J., Wang, W.-X., 2021. Toxicity assessment and underlying mechanisms of multiple metal organic frameworks using the green algae *Chlamydomonas reinhardtii* model. Environ. Pollut. 291, 118199.

Li, Y., Xu, Z., Wang, W.-X., 2022. Effective flocculation of harmful algae *Microcystis aeruginosa* by nanoscale metal–organic framework $NH_2$-MIL-101(Cr). Chem. Eng. J. 433, 134584.

Li, D., Gao, Y., Mu, M., Zhu, S., Zhang, N., Lu, M., 2023. Ionic liquid-modified UiO-66-$NH_2$ as sorbent of dispersive solid-phase extraction for rapid adsorption and enrichment of benzoylurea insecticides. Mirochim. Acta 190, 446.

Liu, S., Lu, Y., Chen, W.J., 2018. Bridge knowledge gaps in environmental health and safety for sustainable development of nano-industries. Nano Today 23, 11–15.

Liu, W., Li, M., Li, W., Keller, A.A., Slaveykova, V., 2022. Metabolic alterations in alga *Chlamydomonas reinhardtii* exposed to $nTiO_2$ materials. Environ. Sci.: Nano 9, 2922–2938.

Majumdar, S., Keller, A.A., 2020. Omics to address the opportunities and challenges of nanotechnology in agriculture. Crit. Rev. Environ. Sci. Technol. 1–42.

Malina, T., Maršálková, E., Holá, K., Tuček, J., Scheibe, M., Zbořil, R., Maršálek, B., 2019. Toxicity of graphene oxide against algae and cyanobacteria: nanoblade-morphology-induced mechanical injury and self-protection mechanism. Carbon 155, 386–396.

Monikh, A.F., Arenas-Lago, D., Porcal, P., Grillo, R., Zhang, P., Guo, Z., Vijver, M.G., Peijnenberg, W.J.G.M., 2020. Do the joint effects of size, shape and ecocorona influence the attachment and physical eco(cyto)toxicity of nanoparticles to algae? Nanotoxicity 14, 310–325.

Monikh, A.F., Chupani, L., Arenas-Lago, D., Guo, Z., Zhang, P., Darbha, G.K., Valsami-Jones, E., Lynch, I., Vijver, M.G., van Bodegom, P., Peijnenburg, W.J.G.M., 2021. Particle number-based trophic transfer of gold nanomaterials in an aquatic food chain. Nat. Commun. 12, 899.

Mu, M., Zhu, S., Gao, Y., Zhang, N., Wang, Y., Lu, M., 2023. Construction of hierarchically porous metal-organic framework HP-UiO-66-30% for sensitive determination of benzoylurea insecticides. Talanta 260, 124540.

Nicholson, J.K., Connelly, J., Lindon, J.C., Holmes, E., 2002. Metabonomics: a platform for studying drug toxicity and gene function. Nat. Rev. Drug Discov. 1, 153–161.

Orellana-Tavra, C., Mercado, S.A., Fairen-Jimenez, D., 2016. Endocytosis mechanism of nano metal-organic frameworks for drug delivery. Adv. Healthc. Mater. 5, 2261–2270.

Patti, G.J., Yanes, O., Siuzdak, G., 2012. Metabolomics: the apogee of the omics trilogy. Nat. Rev. Mol. Cell Biol. 13, 263–269.

Qu, F., Liang, H., He, J., Ma, J., Wang, Z., Yu, H., Li, G., 2012. Characterization of dissolved extracellular organic matter (dEOM) and bound extracellular organic matter (bEOM) of Microcystis aeruginosa and their impacts on UF membrane fouling. Water Res. 46, 2881–2890.

Rego, R.M., Kurkuri, M.D., Kigga, M., 2022. A comprehensive review on water remediation using UiO-66 MOFs and their derivatives. Chemosphere 302, 134845.

Ruyra, À., Yazdi, A., Espín, J., Carné-Sánchez, A., Roher, N., Lorenzo, J., Imaz, I., Maspoch, D., 2015. Synthesis, culture medium stability, and in vitro and in vivo zebrafish embryo toxicity of metal–organic framework nanoparticles. Chem. Eur J. 21, 2508–2518.

Slaveykova, V.I., Majumdar, S., Regier, N., Li, W., Keller, A., 2021. Metabolomic responses of green alga *Chlamydomonas reinhardtii* exposed to sublethal concentrations of inorganic and methylmercury. Environ. Sci. Technol. 55, 3876–3887.

Tortella, G.R., Rubilar, O., Durán, N., Diez, M., Martínez, M., Parada, J., Seabra, A.B., 2020. Silver nanoparticles: toxicity in model organisms as an overview of its hazard for human health and the environment. J. Hazard. Mat. 390, 121974.

Wang, L., Liang, W., Yu, J., Liang, Z., Ruan, L., Zhang, Y., 2013. Flocculation of *Microcystis aeruginosa* using modified larch tannin. Environ. Sci. Technol. 47, 5771–5777.

Wang, S.-C., Liu, G.-Z., Liu, F.-F., 2023. Physiological and metabolic toxicity of polystyrene microplastics to *Dunaliella salina*. Environ. Pollut. 316, 120544.

Wu, B., Torres-Duarte, C., Cole, B.J., Cherr, G.N., 2015. Copper oxide and zinc oxide nanomaterials act as inhibitors of multidrug resistance transport in sea urchin embryos: their role as chemosensitizers. Environ. Sci. Technol. 49, 5760–5770.

Wu, G., Ma, J., Li, S., Wang, S., Jiang, B., Luo, S., Li, J., Wang, X., Guan, Y., Chen, L., 2020. Cationic metal-organic frameworks as an efficient adsorbent for the removal of 2, 4-dichlorophenoxyacetic acid from aqueous solutions. Environ. Res. 186, 109542.

Xin, H., Tang, Y., Liu, S., Yang, X., Xia, S., Yin, D., Yu, S., 2018. Impact of graphene oxide on algal organic matter of *Microcystis aeruginosa*. ACS Omega 3, 16969–16975.

Xiong, J.-Q., Cui, P., Ru, S., Kurade, M.B., Patil, S.M., Yadav, K.K., Fallatah, A.M., Cabral-Pinto, M.M.S., Jeon, B.H., 2022. A comprehensive review on the effects of engineered nanoparticles on microalgal treatment of pollutants from wastewater. J. Clean. Prod. 344, 131121.

Yan, Z., Yang, X., Lynch, I., Cui, F., 2022. Comparative evaluation of the mechanisms of toxicity of graphene oxide and graphene oxide quantum dots to blue-green algae *Microcystis aeruginosa* in the aquatic environment. J. Hazard Mater. 425, 127898.

You, X., Cao, X., Zhang, X., Guo, J., Sun, W., 2021. Unraveling individual and combined toxicity of nano/microplastics and ciprofloxacin to *Synechocystis sp.* at the cellular and molecular levels. Environ. Int. 157, 106842.

Yuan, P., Zhou, Q., Hu, X., 2018. The phases of $WS_2$ nanosheets influence uptake, oxidative stress, lipid peroxidation, membrane damage, and metabolism in algae. Environ. Sci. Technol. 52, 13543–13552.

Yuan, H., Li, J., Pan, L., Li, X., Yuan, Y., Zhong, Q., Wu, X., Luo, J., Yang, S.-T., 2022. Particulate toxicity of metal-organic framework UiO-66 to white rot fungus *Phanerochaete chrysosporium*. Ecotoxicol. Environ. Saf. 247, 114275.

Yue, L., Tao, M., Xu, L., Wang, C., Xu, Y., Liu, Y., Cao, X., White, J.C., Wang, Z., 2023. Size-dependent photocatalytic inactivation of *Microcystis aeruginosa* and degradation of microcystin by a copper metal organic framework. J. Hazard Mater. 462, 132799.

Zhang, W., Song, R., Cao, B., Yang, X., Wang, D., Fu, X., Song, Y., 2018. Variations of floc morphology and extracellular organic matters (EOM) in relation to floc filterability under algae flocculation harvesting using polymeric titanium coagulants (PTCs). Bioresour. Technol. 256, 350–357.

Zhang, X., Hu, X., Wu, H., Mu, L., 2021. Persistence and recovery of ZIF-8 and ZIF-67 phytotoxicity. Environ. Sci. Technol. 55, 15301–15312.

Zhao, X., Xu, M., Song, X., Zhou, W., Liu, X., Yan, Y., Huo, P., 2022. Charge separation and transfer activated by covalent bond in UiO-66-$NH_2$/RGO heterostructure for $CO_2$ photoreduction. Chem. Eng. J. 437, 135210.

Zou, D., Liu, D., 2019. Understanding the modifications and applications of highly stable porous frameworks via UiO-66. Mater. Today Chem. 12, 139–165.